

Double Core-Hole Generation in O₂ Molecules Using an X-Ray Free-Electron Laser: Molecular-Frame Photoelectron Angular Distributions

Gregor Kastirke,¹ Markus S. Schöffler,¹ Miriam Weller,¹ Jonas Rist,¹ Rebecca Boll,² Nils Anders,¹ Thomas M. Baumann,² Sebastian Eckart,¹ Benjamin Erk,³ Alberto De Fanis,² Kilian Fehre,¹ Averell Gatton,⁴ Sven Grundmann,¹ Patrik Grychtol,² Alexander Hartung,¹ Max Hofmann,¹ Markus Ilchen,^{2,5} Christian Janke,¹ Max Kircher,¹ Maksim Kunitski,¹ Xiang Li,⁶ Tommaso Mazza,² Niklas Melzer,¹ Jacobo Montano,² Valerija Music,^{2,5} Giammarco Nalin,¹ Yevheniy Ovcharenko,² Andreas Pier,¹ Nils Rennhack,² Daniel E. Rivas,² Reinhard Dörner,¹ Daniel Rolles,⁶ Artem Rudenko,⁶ Philipp Schmidt,^{2,5} Juliane Siebert,¹ Nico Strenger,¹ Daniel Trabert,¹ Isabel Vela-Perez,¹ Rene Wagner,² Thorsten Weber,⁷ Joshua B. Williams,⁸ Pawel Ziolkowski,² Lothar Ph. H. Schmidt,¹ Achim Czasch,¹ Kiyoshi Ueda,⁹ Florian Trinter,^{3,10} Michael Meyer,² Philipp V. Demekhin,^{5,*} and Till Jahnke^{1,†}

¹Institut für Kernphysik, Goethe-Universität, Max-von-Laue-Strasse 1, 60438 Frankfurt am Main, Germany

²European XFEL GmbH, Holzkoppel 4, 22869 Schenefeld, Germany

³Deutsches Elektronen-Synchrotron (DESY), Notkestrasse 85, 22607 Hamburg, Germany

⁴SLAC National Accelerator Laboratory, Menlo Park, California 94025, USA

⁵Institut für Physik und CINSA, Universität Kassel, Heinrich-Plett-Strasse 40, 34132 Kassel, Germany

⁶J.R. Macdonald Laboratory, Department of Physics, Kansas State University, Manhattan, Kansas 66506, USA

⁷Lawrence Berkeley National Laboratory, Chemical Sciences Division, Berkeley, California 94720, USA

⁸Department of Physics, University of Nevada, Reno, Nevada 89557, USA

⁹Institute of Multidisciplinary Research for Advanced Materials, Tohoku University, Sendai 980-8577, Japan

¹⁰Molecular Physics, Fritz-Haber-Institut der Max-Planck-Gesellschaft, Faradayweg 4-6, 14195 Berlin, Germany



(Received 7 May 2020; accepted 28 August 2020; published 14 October 2020)

We report on a multiparticle coincidence experiment performed at the European X-ray Free-Electron Laser at the Small Quantum Systems instrument using a COLTRIMS reaction microscope. By measuring two ions and two electrons in coincidence, we investigate double core-hole generation in O₂ molecules in the gas phase. Single-site and two-site double core holes have been identified and their molecular-frame electron angular distributions have been obtained for a breakup of the oxygen molecule into two doubly charged ions. The measured distributions are compared to results of calculations performed within the frozen- and relaxed-core Hartree-Fock approximations.

DOI: [10.1103/PhysRevLett.125.163201](https://doi.org/10.1103/PhysRevLett.125.163201)

Photoelectrons emitted from molecules have aroused great interest for many decades. Spectroscopic features providing information on electron binding energies and electronic orbital structures have been investigated, and angular emission distributions were used to gather even more detailed information on orbital angular momentum properties. In particular, electrons emitted from core orbitals are local probes of the bonding and of the nearest atomic neighbors [1], which has made core-hole spectroscopy using synchrotron radiation a widely used tool in molecular physics. In 1987, Cederbaum and co-workers have pointed out that “double core ionization probes the bonding properties much

more sensitively than single core ionization” [2,3], as, for example, the chemical shift of double core-hole states (involving atoms of the same species in a larger molecule) are typically increased as compared to the single core-hole case. They suggested that—given sufficiently high photon intensities—not only one, but two electrons can be emitted from the *K* shell of atoms or molecules. These *K* electrons may be emitted either from the same atom, a case which has been termed single-site double core-hole (SSDCH) generation, or from the *K* shell of different atoms. The latter has been named two-site double core-hole (TSDCH) creation. In both cases, the two *K* vacancies are created before the *K* shell is replenished by an Auger decay, which, in case of small diatomic molecules, typically occurs within less than 5 fs. Ionization schemes where the second *K* electron is emitted after an Auger decay are referred to as photoelectron-Auger electron-photoelectron (PAP) sequences in the literature.

The advent of x-ray free-electron lasers triggered several DCH studies, both theoretically [4–7] and experimentally

Published by the American Physical Society under the terms of the [Creative Commons Attribution 4.0 International license](https://creativecommons.org/licenses/by/4.0/). Further distribution of this work must maintain attribution to the author(s) and the published article's title, journal citation, and DOI. Open access publication funded by the Max Planck Society.

[8–11]. In the XFEL experiments, two electrons were emitted after sequential absorption of two x-ray photons. In parallel to experiments performed at XFELs, detailed spectroscopic studies of DCH states have also been done by employing third-generation synchrotron light sources, which investigated the emission of two electrons after absorption of a single high-energy photon [12,13]. An observation of this ionization scheme is challenging, as the second electron emission is facilitated by electron-electron correlation, which makes it an unlikely process.

The original proposal by Cederbaum *et al.* focused only on the energetics of the DCH creation process—much in line with standard spectroscopy approaches. Today, more advanced experimental tools are at our disposal, which go beyond measuring photoelectron energies and laboratory-frame electron angular distributions. Measurements of electron angular distributions in the molecular frame of reference (molecular-frame photoelectron angular distributions, MFPADs) are performed routinely, nowadays. Such MFPADs are highly sensitive probes of the molecular geometry and potential. Moreover, they are sensitive to electron-electron correlation, selection rules, and nuclear degrees of freedom such as, e.g., stretch and bending modes. The photoelectron wave is launched locally from the respective K shell and then travels through the molecule. On its path it is scattered multiple times in the molecular potential, illuminating the molecule from within [14–16]. For example, the MFPADs of low-energy photoelectrons emitted from the K shell of CH_4 depict directly the three-dimensional molecular structure [17], and in diatomic molecules the bond distance has been mapped by such *photoelectron diffraction* using single-photon ionization [18–21] or strong-field ionization [22]. Close to the ionization threshold, the MFPADs are—as mentioned earlier—also highly sensitive to electron-electron correlations [23], and the presence of doubly excited states is imprinted on the MFPADs [24–26], as well as possibly occurring shape resonances [27,28]. However, the small cross section for the creation of double core vacancies has precluded the observation of their MFPADs, so far. In the present work, we meet that challenge and report the first MFPADs of electrons emitted after SSDCH and TSDCH creation in O_2 .

Any electron angular emission distribution can be naturally expanded in a basis of spherical harmonics $Y_{l,m}$ [29,30], i.e., angular momentum eigenfunctions. The outgoing wave packet can be described as a coherent sum over its partial waves [31]. For the $1s$ photoionization of diatomic molecules (within the dipole approximation) the MFPAD for linearly polarized light is given by

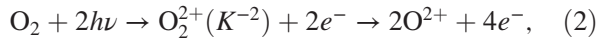
$$\frac{d\sigma}{d\Omega} \sim \left| \cos(\beta) \sum_{l=0} a_{l,0} Y_{l,0} + \sin(\beta) \left(\sum_{l=1} a_{l,+1} Y_{l,+1} + \sum_{l=1} a_{l,-1} Y_{l,-1} \right) \right|^2. \quad (1)$$

Here, β is the angle between the molecular axis and the polarization vector of the ionizing radiation. The first contribution in Eq. (1), which is proportional to $\cos(\beta)$, describes the emission of σ partial waves with $m = 0$, while the second one, proportional to $\sin(\beta)$, represents π partial waves with $m = \pm 1$. Note that, after integration over the molecular orientation angle β , the σ and π contributions add incoherently. Despite the restrictions imposed by the dipole approximation—a single photon deposits only $1\hbar$ of angular momentum into the system—higher angular momentum contributions of the photoelectron can occur. This is possible as these are compensated by a rotational excitation of the molecular ion in order to comply with angular momentum conservation. The latter rotational excitation has been observed, for example, by Choi and co-workers in 1994 [32]. For homonuclear molecules, a further aspect contributes to the molecular-frame angular distributions owing to the nonlocal property of the core hole generated in the photoionization process. Accordingly, the emitted electron wave emerges from a superposition of the molecule’s indistinguishable sites, and the observed emission pattern resembles that of a classical double slit [29,33–36].

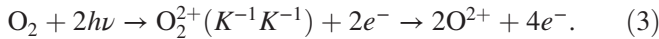
In order to observe MFPADs in an experiment, the orientation of the molecule at the instant of photoionization needs to be known precisely. In gas-phase studies, this can be achieved by determining the orientation from a coincidence measurement. Here, the emission directions of the ionic fragments of the molecule (which are generated, for example, after an Auger decay and a fragmentation of the molecule in a Coulomb explosion subsequent to the initial ionization) are measured in coincidence with the photoelectron emission direction. This provides all information needed to obtain MFPADs if the so-called axial recoil approximation holds (i.e., the molecule does not significantly rotate prior to fragmentation). In our experiment, we employed the COLTRIMS reaction microscope [37–39] available as a permanent end station at the Small Quantum Systems (SQS) instrument of the European X-ray Free-Electron Laser. In brief, a supersonic gas jet is intersected with the x rays forming a well-localized interaction region. Charged particles created in the photoreaction are guided by homogeneous electric (43 V/cm) and magnetic (13.7 G) fields to two time- and position-sensitive micro-channel plate detectors with hexagonal delay-line position readout [40] (active area of 120 mm diameter). The ion and electron arms of the COLTRIMS analyzer had a length of 25.5 cm and 65 cm, respectively. From the flight time and the position of impact on the detector, the initial momentum of each detected particle is determined. Electrons and O^{2+} ions with kinetic energies up to 140 eV and 60 eV, respectively, have been detected with full solid angle coverage. The reaction products of ionization and fragmentation events of individual molecules have been measured in coincidence. The free-electron laser provided

photon pulses with a duration of approximately 25 fs (based on the electron bunch charge of 250 pC) at a photon energy of $h\nu = 670$ eV and pulse energies of $14 \pm 2 \mu\text{J}$ in the interaction region. The latter value considers the assumed beam-line transmission of 0.46 for the selected photon energy and an attenuation of the initial pulse energy of 2.4 mJ to $30 \pm 5 \mu\text{J}$ by using a 15-m-long gas absorber filled with nitrogen. The focus size has been determined using a wave-front sensor (at $h\nu = 1000$ eV) to be $\sim 0.9 \times 1.6 \mu\text{m}^2$. The XFEL's pulse train scheme yielded (due to the constraints imposed by the ions' time-of-flight measurement) an effective repetition rate of up to 420 Hz.

We investigated the SSDCH creation, followed by two Auger decays and Coulomb explosion into two O^{2+} fragments:



and the corresponding TSDCH generation process:



The photon energy of $h\nu = 670$ eV employed in our experiment yielded K photoelectrons of 127 eV. If a second K electron is emitted from the same site as the initial K electron, its kinetic energy is substantially lower. Figure 1 (top) shows the measured electron energy spectrum for the $\text{O}^{2+}/\text{O}^{2+}$ final state. The SSDCH occurs as a small feature at the expected electron energy of 30 eV. A peak at approximately 95 eV results from sequential K -electron emission via the PAP scheme [41], and the main line (the first K emission) is visible at an energy of 127 eV. The TSDCH intensity is located between the PAP feature and the main K line at an energy of about 110 eV. The large amount of low-energy electrons peaking at zero kinetic energy can be attributed to other ionization schemes as double ionization or shakeup ionization with subsequent Auger decays or ionization by Auger cascades.

The middle panel of Fig. 1 shows a coincidence map of the kinetic energies of detected electrons. The coincidence feature of the SSDCH generation (i.e., events of coincident detection of the first and second K photoelectrons) is clearly visible as a small island at energies of (30 eV/127 eV). By constraining the measured dataset to that island, we are able to extract the corresponding molecular-frame photoelectron angular distribution of the second electron emitted in the SSDCH process. The result is shown in Fig. 2(a) as solid circles with error bars and depicts the polarization-averaged MFPAD, i.e., the MFPAD which has been obtained after integrating over all orientations of the molecule in the laboratory frame. We modeled the MFPADs using the stationary single center (SC) method and code [42–44]. The calculations were performed at the equilibrium internuclear geometry of the neutral ground state of the molecule in the frozen- and

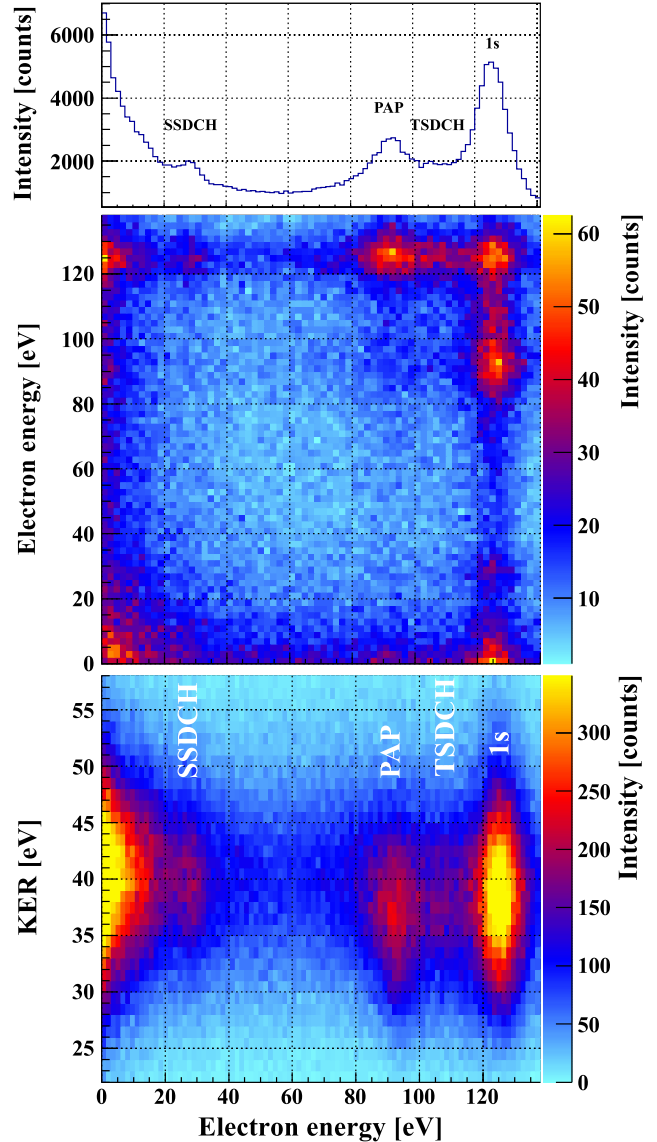


FIG. 1. Photoelectron spectrum and kinetic energy release of O_2 molecules after irradiation with XFEL pulses of $h\nu = 670$ eV at pulse energies of approximately $14 \mu\text{J}$. Only electrons belonging to a final breakup of the molecule into $\text{O}^{2+}/\text{O}^{2+}$ are shown. Top: integrated electron spectrum. Middle: electron energy coincidence map. Bottom: coincidence map of kinetic energy release and electron energy. The intensity axis of the bottom panel has been cropped at 350 (actual maximum value is 520) in order to enhance the visibility of weak features.

relaxed-core Hartree-Fock approximations (FCHF and RCHF). Within the FCHF approximation, the orbitals of the remaining electrons are modeled as frozen in their configuration prior to the photoionization, when generating the potential for the second photoelectron. The RCHF approximation, on the other hand, implies a relaxation of these orbitals to the potential of the core-ionized molecule. The SC expansions of the bound and continuum electrons were restricted by partial waves with $\ell_c \leq 99$ and $\ell_e \leq 49$, respectively. The calculations were performed for the

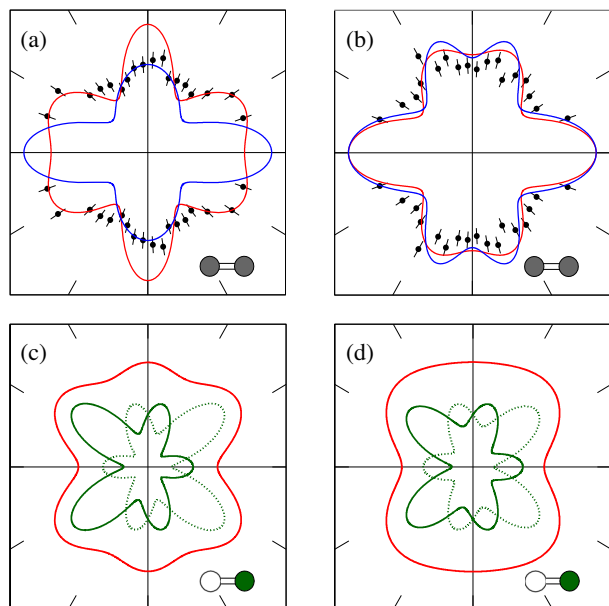


FIG. 2. Polarization-averaged MFPADs of the second electron emitted after (a) SSDCH and (b) TSDCH creation. Symbols with error bars: present experiment. Solid curves: the corresponding results obtained from the theoretical modeling of the process using the frozen-core (blue) and relaxed-core (red) Hartree-Fock approximations. Panels (c) and (d) show the separate contributions to the predicted MFPADs for the emission of the second electron from the right or the left nucleus (solid and dotted curve, respectively), as computed in the relaxed-core Hartree-Fock approximation and for an electron energy of 10 eV (see text).

respective photoelectron kinetic energies mentioned above and averaged over the two contributions for the photoionization of the left and right oxygen atoms. The theoretical results are depicted by blue (frozen-core Hartree-Fock) and red (relaxed-core Hartree-Fock) curves in Fig. 2 on absolute scale to each other, i.e., without any relative rescaling. The measured data have been scaled to best fit the theory. The computational results differ markedly, and the relaxed-core approximation (red curve) agrees considerably better with the measured distribution. In order to understand this difference between the two theoretical results, we performed calculations of the photoionization cross sections of the second K photoelectron. Both approximations predict the occurrence of a σ -shape resonance, albeit at different photoelectron kinetic energies. In the frozen-core Hartree-Fock approximation, the computed cross section for the emission of σ photoelectrons exhibits a broad shape resonance around 40 eV, covering kinetic energies of the second K photoelectron measured for the SSDCH generation process. On molecular shape resonances, the one-particle Hartree-Fock approximation usually fails [30], and contributions from different partial waves start to distinctly alter the computed angular distributions. Indeed, the theoretical MFPAD depicted in Fig. 2(a) by the blue curve (frozen-core Hartree-Fock) exhibits an enhanced

contribution from σ waves, i.e., it overestimates an electron emission along the molecular axis. In contrast, due to the relaxation of the core, the effective charge of the molecular ion saturates toward its asymptotical value of +2 already at shorter distances, yielding a shift of the σ -shape resonance toward higher energies to about 70 eV. This resonance is not affecting the one-particle Hartree-Fock calculations at the kinetic energies around 30 eV, yielding a good agreement between the relaxed-core Hartree-Fock calculations (red curve) and the measured data.

Figure 2(b) shows the polarization-averaged MFPAD of the second photoelectron emitted by the TSDCH generation process. The experimental distribution has been obtained by gating on electrons, which occur in the region of $106 \text{ eV} < E_e < 115 \text{ eV}$ in coincidence with an electron from the main line (middle panel of Fig. 1). While the TSDCH feature is not clearly separable from the PAP feature and the main line, the coincidence map of measured electron energy and kinetic energy release suggests that the energy gate employed here is a valid choice. That map is shown in Fig. 1 (bottom), and it illustrates that the different ionization features appear in ranges of different kinetic energy releases. Accordingly, this map suggests that the contamination of the TSDCH feature by the main line and the PAP contribution is within an acceptable level. The results from our theoretical modeling are shown in Fig. 2(b) by the solid curves. Both, the frozen- and relaxed-core Hartree-Fock approximations yield very similar angular emission distributions which agree very well with the experimental data. This agreement indicates that for the second K photoelectron emitted during the TSDCH generation process, the kinetic energy range of interest (around 110 eV) is free from molecular shape resonances. As pointed out earlier, MFPADs are known to be very sensitive to the exact features of the molecular potential. Thus, the MFPADs of the SSDCH and TSDCH channels might image the inherently different charge distribution of both channels, resulting in more or less asymmetric features. As the final $\text{O}^{2+}/\text{O}^{2+}$ channel is symmetric by definition, any asymmetric features become unobservable in the experiment. However, we can distinguish between the two centers in theory. We, furthermore, chose the same electron energy of 30 eV for the comparison of both channels, as the electron wavelength determines to large amount the shape of the MFPAD. Surprisingly, in the calculation we find the two MFPADs to be almost indistinguishable (not shown). By lowering the electron energy from 30 eV to 10 eV, however, subtle differences emerge. The corresponding SSDCH and TSDCH MFPADs are depicted in Figs. 2(c) and 2(d) with the second electron being emitted from the *right* (green, solid line) or the *left* oxygen atom (white, dotted line). The sum of both is provided by the red line, predicting the symmetrized distribution observable in an experiment. The findings suggest that in order to image the properties of the

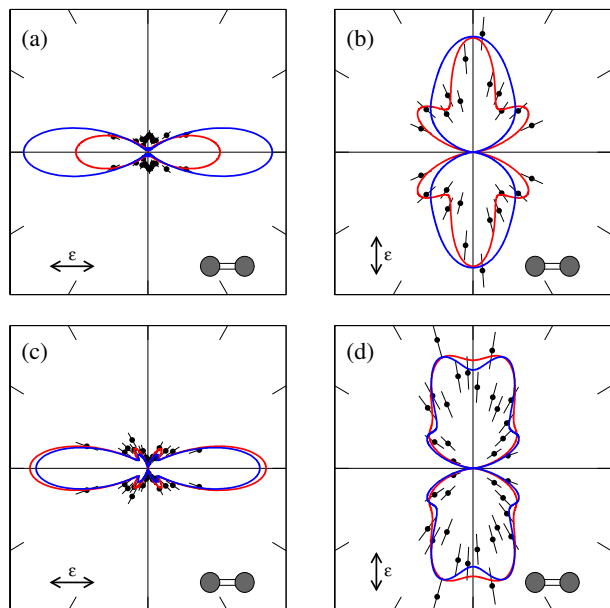


FIG. 3. MFPADs of the second electron emitted after the SSDCH (a),(b) and TSDCH (c),(d) creation for horizontal (left panels) and vertical (right panels) orientation of the molecule with respect to the light polarization axis (see caption of Fig. 2 for details on the data presentation).

molecular potential connected to the exact charge of its atoms, electrons of even lower energies need to be employed.

Finally, Fig. 3 depicts the computed and measured MFPADs for different orientations of the molecular axis with respect to the polarization direction of the ionizing light. The two panels on the left show the MFPADs for σ orientation and those on the right the corresponding MFPADs for π orientation. In the σ case, the molecule is aligned within $\pm 15^\circ$ with respect to the photons' polarization vector. The π case corresponds to an alignment within $\pm 15^\circ$ perpendicular to the polarization axis. Furthermore, the electron emission angles are restricted in the latter case to the plane spanned by the polarization vector and the molecule with an opening angle of $\pm 15^\circ$, as well. The same normalization procedure as in Fig. 2 has been applied. The angular distributions shown in panel (a) fortify the assumptions concerning a shape resonance in one of the theoretical models as the frozen-core Hartree-Fock approximation (blue curve) significantly overestimates the contribution from σ waves. The π contributions computed for the SSDCH photoelectrons [Fig. 3(b)] and both σ and π contributions computed for the TSDCH photoelectrons [Figs. 3(c) and 3(d)] do not differ significantly for the frozen- and relaxed-core potentials, and are in a good agreement with the corresponding experimental results.

In conclusion, we have presented first molecular-frame photoelectron angular distributions of the second electron emitted by double core-hole creation in O_2 molecules.

These results are, to the best of our knowledge, the first two-electron-two-ion coincidence measurements of that kind. Future measurements of this type might be employed to observe electron dynamics on the attosecond scale, as proposed very recently [45]. Results for single-site and two-site DCH generation have been shown. The respective MFPADs were modeled theoretically within the frozen-core and relaxed-core Hartree-Fock approximations. In the case of TSDCH, the two approximations yield very similar angular emission distributions, which are both in good agreement with the measured data. For SSDCH creation, the relaxed-core Hartree-Fock approximation results in a good agreement between theory and experiment, while the frozen-core Hartree-Fock approximation fails. This happens because in the latter approximation, the σ -shape resonance of the second photoelectron occurs at the kinetic energies where the second SSDCH photoelectrons are observed in the experiment.

We acknowledge European XFEL in Schenefeld, Germany, for provision of x-ray free-electron laser beam time at the SQS instrument and would like to thank the staff for their assistance. We are indebted to A. Bräuning-Demian for timely support during the beamtime preparations. This work has been supported by the Bundesministerium für Bildung und Forschung (BMBF), Grants No. 05K13RF4 and No. 05K16RF1. The theoretical work was supported by the DFG Project No. DE 2366/1-2. M. S. S., S. G., K. F., and R. D. acknowledge support from Deutsche Forschungsgemeinschaft via Sonderforschungsbereich 1319 (ELCH). M. I., Ph. S., and V. M. acknowledge funding by the Volkswagen foundation within a Peter Paul Ewald-Fellowship. K. U. acknowledges funding by the Dynamic Alliance for Open Innovation Bridging Human, Environment and Materials" and the "IMRAM (Institute of Multidisciplinary Research for Advanced Materials) project." Th. W. was supported by the U.S. Department of Energy Office of Basic Energy Sciences, Division of Chemical Sciences, Biosciences, and Geosciences under contract No. DE-AC02-05CH11231. X. L, D. R., and A. R. are supported by the Chemical Sciences, Geosciences, and Biosciences Division, Office of Basic Energy Sciences, Office of Science, U.S. Department of Energy, Grant No. DE-SC0019451. J. B. W. acknowledges funding by National Science Foundation Grant No. NSF-PHY-1807017.

*demekhin@physik.uni-kassel.de

†jahnke@atom.uni-frankfurt.de

- [1] K. Siegbahn, C. Nordling, G. Johansson, J. Hedman, P. F. Heden, K. Hamrin, U. Gelius, T. Bergmark, L. O. Werme, R. Manne, and Y. Baer, *ESCA Applied to Free Molecules* (North-Holland Pub. Co, Amsterdam, 1969).
- [2] L. S. Cederbaum, F. Tarantelli, A. Sgamellotti, and J. Schirmer, *J. Chem. Phys.* **86**, 2168 (1987).

- [3] L. S. Cederbaum, F. Tarantelli, A. Sgamellotti, and J. Schirmer, *J. Chem. Phys.* **85**, 6513 (1986).
- [4] R. Santra, N. V. Kryzhevoi, and L. S. Cederbaum, *Phys. Rev. Lett.* **103**, 013002 (2009).
- [5] M. Tashiro, M. Ehara, H. Fukuzawa, K. Ueda, C. Buth, N. V. Kryzhevoi, and L. S. Cederbaum, *J. Chem. Phys.* **132**, 184302 (2010).
- [6] M. Tashiro, M. Ehara, and K. Ueda, *Chem. Phys. Lett.* **496**, 217 (2010).
- [7] O. Takahashi, M. Tashiro, M. Ehara, K. Yamasaki, and K. Ueda, *J. Chem. Phys. A* **115**, 12070 (2011).
- [8] J. P. Cryan *et al.*, *Phys. Rev. Lett.* **105**, 083004 (2010).
- [9] L. Fang, M. Hoener, O. Geßner, F. Tarantelli, S. T. Pratt, O. Kornilov, C. Buth, M. Gühr, E. P. Kanter, C. Bostedt, J. D. Bozek, P. H. Bucksbaum, M. Chen, R. Coffee, J. Cryan, M. Glowonia, E. Kukk, S. R. Leone, and N. Berrah, *Phys. Rev. Lett.* **105**, 083005 (2010).
- [10] N. Berrah, L. Fang, B. Murphy, T. Osipov, K. Ueda, E. Kukk, R. Feifel, P. van der Meulen, P. Salen, H. T. Schmidt, R. D. Thomas, M. Larsson, R. Richter, K. C. Prince, J. D. Bozek, C. Bostedt, S. Wada, M. N. Piancastelli, M. Tashiro, and M. Ehara, *Proc. Natl. Acad. Sci. U.S.A.* **108**, 16912 (2011).
- [11] P. Salén, P. van der Meulen, H. T. Schmidt, R. D. Thomas, M. Larsson, R. Feifel, M. N. Piancastelli, L. Fang, B. Murphy, T. Osipov, N. Berrah, E. Kukk, K. Ueda, J. D. Bozek, C. Bostedt, S. Wada, R. Richter, V. Feyer, and K. C. Prince, *Phys. Rev. Lett.* **108**, 153003 (2012).
- [12] J. H. D. Eland, M. Tashiro, P. Linusson, M. Ehara, K. Ueda, and R. Feifel, *Phys. Rev. Lett.* **105**, 213005 (2010).
- [13] P. Lablanquie, F. Penet, J. Palaudoux, L. Andric, P. Selles, S. Carniato, K. Bučar, M. Žitnik, M. Huttula, J. H. D. Eland, E. Shigemasa, K. Soejima, Y. Hikosaka, I. H. Suzuki, M. Nakano, and K. Ito, *Phys. Rev. Lett.* **106**, 063003 (2011).
- [14] A. Landers, Th. Weber, I. Ali, A. Cassimi, M. Hattass, O. Jagutzki, A. Nauert, T. Osipov, A. Staudte, M. H. Prior, H. Schmidt-Böcking, C. L. Cocke, and R. Dörner, *Phys. Rev. Lett.* **87**, 013002 (2001).
- [15] H. Fukuzawa, R. R. Lucchese, X.-J. Liu, K. Sakai, H. Iwayama, K. Nagaya, K. Kreidi, M. S. Schöffler, J. R. Harries, Y. Tamenori, Y. Morishita, I. H. Suzuki, N. Saito, and K. Ueda, *J. Chem. Phys.* **150**, 174306 (2019).
- [16] H. Fukuzawa, S. Yamada, Y. Sakakibara, T. Tachibana, Y. Ito, T. Takanashi, T. Nishiyama, T. Sakai, K. Nagaya, N. Saito, M. Oura, M. Stener, P. Decleva, and K. Ueda, *J. Chem. Phys.* **151**, 104302 (2019).
- [17] J. B. Williams, C. S. Trevisan, M. S. Schöffler, T. Jahnke, I. Bocharova, H. Kim, B. Ulrich, R. Wallauer, F. Sturm, T. N. Rescigno, A. Belkacem, R. Dörner, Th. Weber, C. W. McCurdy, and A. L. Landers, *Phys. Rev. Lett.* **108**, 233002 (2012).
- [18] U. Becker, O. Geßner, and A. Rüdél, *J. Electron Spectrosc. Relat. Phenom.* **108**, 189 (2000).
- [19] D. Rolles, Scattering and coherence phenomena in the photoionization of small molecules, Ph.D. thesis, 2005.
- [20] K. Kreidi *et al.*, *Phys. Rev. Lett.* **100**, 133005 (2008).
- [21] M. S. Schöffler *et al.*, *Phys. Rev. A* **78**, 013414 (2008).
- [22] M. Kunitski, N. Eicke, P. Huber, J. Köhler, S. Zeller, J. Voigtsberger, N. Schlott, K. Henrichs, H. Sann, F. Trinter, L. Ph. H. Schmidt, A. Kalinin, M. S. Schöffler, T. Jahnke, M. Lein, and R. Dörner, *Nat. Commun.* **10**, 1 (2019).
- [23] N. A. Cherepkov, S. K. Semenov, Y. Hikosaka, K. Ito, S. Motoki, and A. Yagishita, *Phys. Rev. Lett.* **84**, 250 (2000).
- [24] M. Lebeck, J. C. Houver, D. Dowek, and R. R. Lucchese, *Phys. Rev. Lett.* **96**, 073001 (2006).
- [25] F. Martín, J. Fernández, T. Havermeier, L. Foucar, Th. Weber, K. Kreidi, M. Schöffler, L. Schmidt, T. Jahnke, O. Jagutzki, A. Czasch, E. P. Benis, T. Osipov, A. L. Landers, A. Belkacem, M. H. Prior, H. Schmidt-Böcking, C. L. Cocke, and R. Dörner, *Science* **315**, 629 (2007).
- [26] A. V. Golovin, F. Heiser, C. J. K. Quayle, P. Morin, M. Simon, O. Geßner, P.-M. Guyon, and U. Becker, *Phys. Rev. Lett.* **79**, 4554 (1997).
- [27] E. Shigemasa, J. Adachi, K. Soejima, N. Watanabe, A. Yagishita, and N. A. Cherepkov, *Phys. Rev. Lett.* **80**, 1622 (1998).
- [28] T. Jahnke *et al.*, *Phys. Rev. Lett.* **88**, 073002 (2002).
- [29] I. G. Kaplan and A. P. Markin, *Dokl. Akad. Nauk SSSR* **184**, 66 (1969).
- [30] J. L. Dehmer and D. Dill, *Phys. Rev. Lett.* **35**, 213 (1975).
- [31] N. A. Cherepkov, *J. Phys. B* **14**, 2165 (1981).
- [32] H. C. Choi, R. M. Rao, A. G. Mihill, S. Kakar, E. D. Poliakoff, K. Wang, and V. McKoy, *Phys. Rev. Lett.* **72**, 44 (1994).
- [33] D. Akoury *et al.*, *Science* **318**, 949 (2007).
- [34] J. Fernandez, O. Fojon, A. Palacios, and F. Martin, *Phys. Rev. Lett.* **98**, 043005 (2007).
- [35] D. Rolles, M. Braune, S. Cvejanovic, O. Geßner, R. Hentges, S. Korica, B. Langer, T. Lischke, G. Prümper, A. Reinköster, J. Viefhaus, B. Zimmermann, V. McKoy, and U. Becker, *Nature (London)* **437**, 711 (2005).
- [36] B. Zimmermann, D. Rolles, B. Langer, R. Hentges, M. Braune, S. Cvejanovic, O. Geßner, F. Heiser, S. Korica, T. Lischke, A. Reinköster, J. Viefhaus, R. Dörner, V. McKoy, and U. Becker, *Nat. Phys.* **4**, 649 (2008).
- [37] J. Ullrich, R. Moshhammer, A. Dorn, R. Dörner, L. Ph. H. Schmidt, and H. Schmidt-Böcking, *Rep. Prog. Phys.* **66**, 1463 (2003).
- [38] R. Dörner, V. Mergel, O. Jagutzki, L. Spielberger, J. Ullrich, R. Moshhammer, and H. Schmidt-Böcking, *Phys. Rep.* **330**, 95 (2000).
- [39] T. Jahnke, Th. Weber, T. Osipov, A. L. Landers, O. Jagutzki, L. Ph. H. Schmidt, C. L. Cocke, M. H. Prior, H. Schmidt-Böcking, and R. Dörner, *J. Electron Spectrosc. Relat. Phenom.* **141**, 229 (2004).
- [40] O. Jagutzki, V. Mergel, K. Ullmann-Pfleger, L. Spielberger, U. Spillmann, R. Dörner, and H. Schmidt-Böcking, *Nucl. Instrum. Methods Phys. Res., Sect. A* **477**, 244 (2002).
- [41] G. Kastirke *et al.*, *Phys. Rev. X* **10**, 021052 (2020).
- [42] Ph. V. Demekhin, A. Ehresmann, and V. L. Sukhorukov, *J. Chem. Phys.* **134**, 024113 (2011).
- [43] Ph. V. Demekhin, D. V. Omel'yanenko, B. M. Lagutin, V. L. Sukhorukov, L. Werner, A. Ehresmann, K.-H. Scharfner, and H. Schmoranzner, *Opt. Spectrosc.* **102**, 318 (2007).
- [44] S. A. Galitskiy, A. N. Artemyev, K. Jänkälä, B. M. Lagutin, and Ph. V. Demekhin, *J. Chem. Phys.* **142**, 034306 (2015).
- [45] L. Inhester, L. Greenman, A. Rudenko, D. Rolles, and R. Santra, *J. Chem. Phys.* **151**, 054107 (2019).